

# Integrated Monostatic and Bistatic mmWave Sensing

Yu Ge\*, Hyowon Kim<sup>†</sup>, Lennart Svensson\*, Henk Wymeersch\*, Sumei Sun<sup>‡</sup>

\*Department of Electrical Engineering, Chalmers University of Technology, Gothenburg, Sweden,

<sup>†</sup>Department of Electronics Engineering, Chungnam National University of Technology, Daejeon, South Korea,

<sup>‡</sup>Institute for Infocomm Research, Agency for Science, Technology and Research, Singapore,

{yuge, lennart.svensson, henkw}@chalmers.se, hyowon.kim@cnu.ac.kr, sunsm@i2r.a-star.edu.sg

**Abstract**—Millimeter-wave (mmWave) signals provide attractive opportunities for sensing due to their inherent geometrical connections to physical propagation channels. Two common modalities used in mmWave sensing are monostatic and bistatic sensing, which are usually considered separately. By integrating these two modalities, information can be shared between them, leading to improved sensing performance. In this paper, we investigate the integration of monostatic and bistatic sensing in a 5G mmWave scenario, implement the extended Kalman-Poisson multi-Bernoulli sequential filters to solve the sensing problems, and propose a method to periodically fuse user states and maps from two sensing modalities.

**Index Terms**—MmWave, monostatic sensing, bistatic sensing, integration, extended Kalman-Poisson multi-Bernoulli filter.

## I. INTRODUCTION

Integrated sensing and communication (ISAC) is expected to be one of the key features of 6G wireless systems [1], and sensing using millimeter-wave (mmWave) signals is at the heart of ISAC. Sensing is a broad term and covers everything from channel estimation and carrier sensing to device localization and environment awareness [2]. The term sensing, in this paper, is referred to the state estimation of the user equipment (UE) and passive objects in the propagation environment, termed as *positioning* and *mapping*, respectively.

Monostatic sensing and bistatic sensing are the two most common sensing modalities [3]. In monostatic sensing, the transmitter and receiver are co-located (or connected with fiber and act as distributed monostatic system), and thus share complete knowledge of the transmitted signals and the clock [3]–[5]. In bistatic sensing, on the other hand, the transmitter and the receiver are usually at different locations, where the receiver may only have partial knowledge of the transmitted signals and the synchronization problem between the transmitter and the receiver needs to be considered [3]–[5]. Fig. 1 provides visualizations of both sensing modalities. Although the two modalities can be employed simultaneously, most existing works only consider one of them.

The related works can be divided into works that solve monostatic and bistatic mmWave sensing problems and works that integrate sensing modalities. The sensing problem (mapping and positioning in this paper) has been studied in many papers and addressed by different approaches [6]–[11]. Among these methods, random finite set (RFS)-based methods [9]–[11] and certain message passing-based methods [8] can

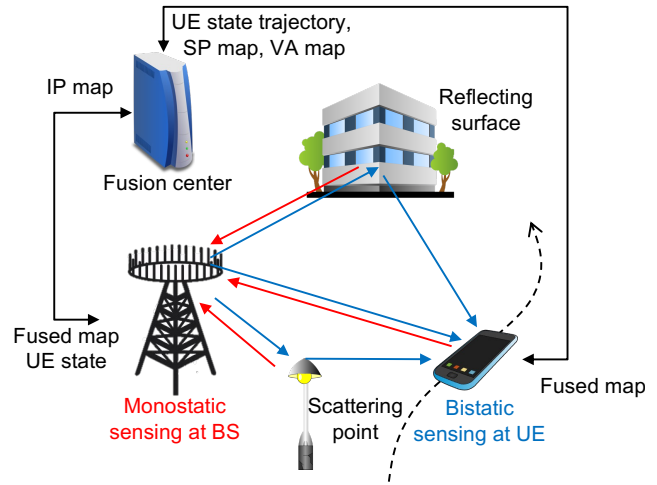


Fig. 1. An example of monostatic sensing and bistatic sensing. In monostatic sensing, the BS sends out signals (in blue), which go through the complex propagation environment and are received back again by the BS (in red), which is then used for sensing. In bistatic sensing, the BS sends signals to the receiver, and those signals go via a complex propagation environment and then reach the UE (in blue), which is then used for sensing. Two sensing modalities are fused and overwritten by the fused map and UE state periodically.

handle the inherent challenges of unknown data associations (DAs), the unknown number of objects/targets, misdetections, and clutter measurements, which all sensing applications with multiple objects/targets suffer from. Within these RFS-based methods, [11] proposed a Poisson multi-Bernoulli (PMB)-based algorithm that can keep both a good sensing performance and an acceptable computational complexity, making it suitable to be used in solving sensing problems. However, only one sensing modality is considered in these works. The integration of sensing modalities is not a new idea and has been considered in earlier literature [4], [5], [12], [13], but they solely consider the integration of several monostatic sensors or several bistatic sensors, not the combination of monostatic and bistatic sensing. The only exception is [14], which proposed a message-passing-based algorithm that fused both sensing modalities in communication systems. However, [14] assumes perfect synchronization between UE and base station (BS), considers the UE orientation to be known, and performs both monostatic and bistatic sensing at the UE side, all of which make the problem considerably easier.

In this paper, we study the integration of monostatic and bistatic sensing to improve the sensing performances and con-

sider a scenario where monostatic sensing is performed by the BS and bistatic sensing is performed at the UE, and clock bias and the UE orientation are estimated. The main contributions of this paper are summarized as follows: (i) we develop an RFS-based integration algorithm that can fuse the UE states and maps from monostatic and bistatic sensing together, and provide the executable details on the proposed method; (ii) we extend our previous work of the extended Kalman (EK)-PMB simultaneous localization and mapping (SLAM) filter in [11] by periodically replacing the corresponding updated maps and UE states with the fused ones; (iii) we validate the benefits of the integrating two sensing modalities through simulations in the mmWave radio network context, and show the integration can significantly enhance sensing performances.

*Notations:* Scalars (e.g.,  $x$ ) are denoted in italics, vectors (e.g.,  $\mathbf{x}$ ) in bold lower-case letters, matrices (e.g.,  $\mathbf{X}$ ) in bold capital letters, and sets (e.g.,  $\mathcal{X}$ ) in calligraphic. Transpose is denoted by  $(\cdot)^\top$ . A Gaussian density with mean  $\mathbf{u}$  and covariance  $\Sigma$ , evaluated at  $\mathbf{x}$ , is denoted by  $\mathcal{N}(\mathbf{x}; \mathbf{u}, \Sigma)$ .

## II. MODELS FOR BISTATIC AND MONOSTATIC SENSING

We consider a scenario where monostatic and bistatic sensing happen at the same time, but the former is by the BS and the latter is by the UE. In this section, we introduce the state models, the received signal models with multiple-input multiple-output (MIMO)-orthogonal frequency-division multiplexing (OFDM) signals, and the measurement models.

### A. State Models

The dynamic state of the UE at time step  $k$ , denoted as  $\mathbf{s}_k$ , consists of the 3D UE position  $\mathbf{x}_{\text{UE},k} = [x_k, y_k, z_k]^\top$ , the heading  $\varpi_k$  and the clock bias  $b_k$  (with respect to the BS). The UE evolves according to state dynamics, and the transition density is given by

$$f(\mathbf{s}_{k+1}|\mathbf{s}_k) = \mathcal{N}(\mathbf{s}_{k+1}; \mathbf{v}(\mathbf{s}_k), \mathbf{Q}_{k+1}), \quad (1)$$

where  $\mathbf{v}(\cdot)$  denotes the known transition function and  $\mathbf{Q}_{k+1}$  is the process noise covariance. In the environment, three types of landmarks are considered, i.e., the BS, scattering points (SPs), and reflecting surfaces. The BS is deployed with a uniform rectangular array (URA), and is parameterized by a location  $\mathbf{x}_{\text{BS}} \in \mathbb{R}^3$ , which is a prior known. A SP, corresponding to a small object, e.g., a street lamp, a traffic sign, etc, is parameterized by a location  $\mathbf{x}_{\text{SP}} \in \mathbb{R}^3$ . A reflecting surface, corresponding to a large surface, e.g., wall, building facade, etc, is parameterized by a fixed virtual anchor (VA) with location  $\mathbf{x}_{\text{VA}} \in \mathbb{R}^3$ . The VA is surface-specific, which is the reflection of the BS with respect to the reflecting surface, given by [15]

$$\mathbf{x}_{\text{VA}} = (\mathbf{I} - 2\nu\nu^\top)\mathbf{x}_{\text{BS}} + 2\boldsymbol{\mu}^\top\nu\nu, \quad (2)$$

where  $\nu$  is the normal to the surface, and  $\boldsymbol{\mu}$  is an arbitrary point on the surface.

There are some differences in how the state models are treated in bistatic and monostatic sensing:

- *Bistatic sensing:* In bistatic sensing, a VA always remains static, even though the incidence point (IP) of the signal,

where the signal hits the landmark, is moving while the UE is moving.

- *Monostatic sensing:* In monostatic sensing, the BS is not aware of the UE dynamics and can only determine the 3D position  $\mathbf{x}_{\text{UE},k}$ . Therefore, the UE is modeled as a random walk with the transition density

$$f(\mathbf{x}_{\text{UE},k+1}|\mathbf{x}_{\text{UE},k}) = \mathcal{N}(\mathbf{x}_{\text{UE},k+1}; \mathbf{x}_{\text{UE},k}, \mathbf{Q}_{k+1}), \quad (3)$$

where  $\mathbf{Q}_{k+1}$  is the (large) process noise covariance. Moreover, as the BS is always fixed, the IPs do not change over time, and there is no difference between small objects and large surfaces. The environment is parameterized using IPs  $\mathbf{x}_{\text{IP}} \in \mathbb{R}^3$  for all landmarks. Please note that the SP is the same as IP for a small object, and the VA can be calculated from the IP

$$\mathbf{x}_{\text{VA}} = 2\mathbf{x}_{\text{IP}} - \mathbf{x}_{\text{BS}}. \quad (4)$$

### B. Signal Models

The BS sends downlink OFDM pilot signals to the UE every time step. These signals are denoted by  $\mathbf{f}_{\text{BS},g,k}x_{\kappa,g}$ , for time step  $k$ , transmission  $g$ , and subcarrier  $\kappa$ , in which  $x_{\kappa,g}$  is the pilot signal and  $\mathbf{f}_{\text{BS},g,k}$  is the precoder at BS. These signals are received by the UE for bistatic sensing and by the BS for monostatic sensing.

1) *Bistatic Sensing:* The downlink signal can reach the UE via the line-of-sight (LoS) path or non-line-of-sight (NLoS) paths, or both, leading to the following observation model [16]

$$y_{\kappa,g,k} = \mathbf{w}_{\text{UE},g,k}^H \sum_{i=1}^{I_k} \rho_k^i \mathbf{a}_{\text{UE}}(\boldsymbol{\theta}_k^i) \mathbf{a}_{\text{BS}}^H(\boldsymbol{\phi}_k^i) e^{-j2\pi\kappa\Delta_f\tau_k^i} \mathbf{f}_{\text{BS},g,k}x_{\kappa,g} + \mathbf{w}_{\text{UE},g,k}^H \mathbf{n}_{\kappa,g,k}, \quad (5)$$

where  $y_{\kappa,g,k}$  is the received signal,  $\mathbf{n}_{\kappa,g,k}$  is the noise,  $\mathbf{w}_{\text{UE},g,k}$  is the combining matrix at the UE side,  $\Delta_f$  is the subcarrier spacing,  $\mathbf{a}_{\text{UE}}(\cdot)$  and  $\mathbf{a}_{\text{BS}}(\cdot)$  are the steering vectors of the UE and the BS antenna arrays, respectively. There are  $I_k$  visible landmarks for bistatic sensing, and we assume that each landmark creates only one path, thus, there are  $I_k$  paths in total. Each path  $i$  can be described by a complex gain  $\rho_k^i$ , a time-of-arrival (ToA)  $\tau_k^i$ , an angle-of-arrival (AoA) pair  $\boldsymbol{\theta}_k^i$  in azimuth and elevation, and an angle-of-departure (AoD) pair  $\boldsymbol{\phi}_k^i$  in azimuth and elevation. The path parameters are related to the geometry, e.g.,  $\tau_k^i = \|\mathbf{x}_{\text{UE},k} - \mathbf{x}_{\text{BS}}\|/c + b_k$  for the LoS path and  $\tau_k^i = \|\mathbf{x}_{\text{UE},k} - \mathbf{x}_{\text{IP}}\|/c + \|\mathbf{x}_{\text{BS}} - \mathbf{x}_{\text{IP}}\|/c + b_k$  for any NLoS path. The relations between AoA/AoD and the geometric state can be found in [17, App. A].

2) *Monostatic Sensing:* The downlink signal is reflected by the reflecting surfaces or diffused by SPs and/or the passive UE back to the BS. Therefore, there is no LoS path in monostatic sensing, and only NLoS paths need to be considered. The observation becomes<sup>1</sup>

$$r_{\kappa,g,k} = \mathbf{w}_{\text{BS},g,k}^H \sum_{i=1}^{L_k} \varrho_k^i \mathbf{a}_{\text{BS}}(\boldsymbol{\vartheta}_k^i) \mathbf{a}_{\text{BS}}^H(\boldsymbol{\vartheta}_k^i) e^{-j2\pi\kappa\Delta_f\epsilon_k^i} \mathbf{f}_{\text{BS},g,k}x_{\kappa,g} + \mathbf{w}_{\text{BS},g,k}^H \mathbf{t}_{\kappa,g,k}, \quad (6)$$

<sup>1</sup>Doppler measurements are not considered due to short transmission periods. However, the inclusion of Doppler measurements would greatly facilitate the detection and estimation of the mobile UE.

where  $r_{\kappa,g,k}$  is the received signal across the BS array,  $\mathbf{t}_{\kappa,g,k}$  is the noise across the BS array,  $\mathbf{w}_{\text{BS},g,k}$  is the combining matrix at the BS side,  $L_k$  is the number of landmarks (including the passive UE) for monostatic sensing. Similar to bistatic sensing, each path  $i$  can also be described by a complex gain  $\varrho_k^i$ , a ToA  $\varepsilon_k^i$ , and an AoA pair  $\vartheta_k^i$  (which is equal to the corresponding AoD). Note that since the BS is synchronized with itself,  $\varepsilon_k^i = 2\|\mathbf{x}_{\text{IP}} - \mathbf{x}_{\text{BS}}\|/c$ , for IPs.

### C. Measurement Models

The channel parameters of ToA, AoA, and AoD of the two sensing modalities can be obtained by applying a channel estimator, e.g., [18]–[21], on (5) and (6) at the UE and BS sides, respectively. However, the channel estimation is beyond the scope of this paper, and the channel parameters are already available to be utilized as measurements for bistatic and monostatic sensing purposes. Measurements provided by the channel estimator at time step  $k$  are modeled as RFSs, given by  $\mathcal{Z}_k^{\text{B}} = \{\mathbf{z}_k^1, \dots, \mathbf{z}_k^{\hat{L}_k}\}$  and  $\mathcal{Z}_k^{\text{M}} = \{\mathbf{z}_k^1, \dots, \mathbf{z}_k^{\hat{L}_k}\}$  for bistatic and monostatic sensing, respectively. Please note that  $\hat{L}_k \neq L_k$  and  $\hat{L}_k \neq L_k$  in general, as some measurements can be clutter which are originated from noise peaks during channel estimation or transient objects, and landmarks might be misdeteected. It is also important to notice that the DA problem is unsolved, which means the source of each measurement is still unclear. The likelihoods differ in monostatic and bistatic sensing, in the following way:

- *Bistatic sensing*: For any  $\mathbf{z}^i \in \mathcal{Z}_k^{\text{B}}$  originating from landmark with IP location  $\mathbf{x}^i$ , the likelihood function is modeled by

$$f(\mathbf{z}_k^i | \mathbf{x}^i, \mathbf{s}_k) = \mathcal{N}(\mathbf{z}_k^i; \mathbf{h}(\mathbf{x}^i, \mathbf{s}_k), \mathbf{R}_k^i), \quad (7)$$

where  $\mathbf{h}(\mathbf{x}^i, \mathbf{s}_k) = [\tau_k^i, (\boldsymbol{\theta}_k^i)^\top, (\boldsymbol{\phi}_k^i)^\top]^\top$  represents the nonlinear function that transforms the geometric information to channel parameters, and  $\mathbf{R}_k^i$  is the measurement covariance determined by the Fisher information matrix (FIM) of channel parameters, as in [22].

- *Monostatic sensing*: For any  $\mathbf{z}_k^i \in \mathcal{Z}_k^{\text{M}}$  originating from a landmark with IP location  $\mathbf{x}^i$ , the likelihood function is modeled by

$$f(\mathbf{z}_k^i | \mathbf{x}^i, \mathbf{s}_k) = \mathcal{N}(\mathbf{z}_k^i; \mathbf{h}(\mathbf{x}^i, \mathbf{x}_{\text{BS}}), \mathbf{R}_k^i), \quad (8)$$

where  $\mathbf{h}(\mathbf{x}^i, \mathbf{x}_{\text{BS}}) = [\varepsilon_k^i, (\boldsymbol{\vartheta}_k^i)^\top]^\top$  denotes the corresponding nonlinear function, and  $\mathbf{R}_k^i$  denotes the measurement covariance.

## III. FILTERS FOR MAPPING AND SLAM AT BS AND UE

In this section, we describe the form of the filter used for mapping the environment and how it is combined with tracking the UE state. The map is modeled as a PMB RFS. In this section, the PMB density and the PMB filters are briefly introduced. Details on the implementation of the filters are outside the scope of this paper, but can be found in [11], [23]–[25].

### A. Basics of PMB Density

We assume a map  $\mathcal{X} = \{\mathbf{x}^1, \dots, \mathbf{x}^{|\mathcal{X}|}\}$  is a PMB RFS. A PMB RFS consists of two disjoint RFSs, a set  $\mathcal{X}_{\text{U}}$  of undetected objects, which are all landmarks that have never been detected before, and a set  $\mathcal{X}_{\text{D}}$  of detected objects, which are landmarks that have been detected at least once before [24]. We model  $\mathcal{X}_{\text{U}}$  as a Poisson point process (PPP) and  $\mathcal{X}_{\text{D}}$  as a multi-Bernoulli (MB), with the following densities

$$f_{\text{P}}(\mathcal{X}_{\text{U}}) = e^{-\int \lambda(\mathbf{x}') d\mathbf{x}'} \prod_{\mathbf{x} \in \mathcal{X}_{\text{U}}} \lambda(\mathbf{x}), \quad (9)$$

$$f_{\text{MB}}(\mathcal{X}_{\text{D}}) = \sum_{\mathcal{X}^1 \uplus \dots \uplus \mathcal{X}^{|\mathcal{X}_{\text{D}}|} = \mathcal{X}_{\text{D}}} \prod_{i=1}^{|\mathcal{X}_{\text{D}}|} f_{\text{B}}^i(\mathcal{X}^i), \quad (10)$$

where  $\lambda(\mathbf{x}) = \eta f_{\text{P}}(\mathbf{x})$  is the intensity function with  $\eta$  denoting the mean of the Poisson distribution and  $f_{\text{P}}(\mathbf{x})$  denoting the spatial density;  $\uplus$  is the union of mutually disjoint sets;  $f_{\text{B}}^i(\cdot)$  is the Bernoulli density of the  $i$ -th landmark, following

$$f_{\text{B}}^i(\mathcal{X}^i) = \begin{cases} 1 - r^i & \mathcal{X}^i = \emptyset \\ r^i f^i(\mathbf{x}) & \mathcal{X}^i = \{\mathbf{x}\} \\ 0 & \text{otherwise,} \end{cases} \quad (11)$$

where  $r^i \in [0, 1]$  is the existence probability, describing how likely the landmark exists, and  $f^i(\cdot)$  is the corresponding spatial density. As  $\mathcal{X}$  is the union of  $\mathcal{X}_{\text{U}}$  and  $\mathcal{X}_{\text{D}}$ , the density of  $\mathcal{X}$  can be computed using the convolution formula [26, eq. (4.17)] as  $f(\mathcal{X}) = \sum_{\mathcal{X}_{\text{U}} \uplus \mathcal{X}_{\text{D}} = \mathcal{X}} f_{\text{P}}(\mathcal{X}_{\text{U}}) f_{\text{MB}}(\mathcal{X}_{\text{D}})$ , which can be parameterized by its components, i.e.,  $\lambda(\mathbf{x})$  and  $\{r^i, f^i(\mathbf{x})\}_{i \in \mathbb{I}}$ , with  $\mathbb{I}$  representing the index set of  $\mathcal{X}_{\text{D}}$ .

### B. PMB-based Filters for Bistatic and Monostatic Sensing

Two different PMB-based filters are implemented independently. A PMB SLAM filter is run at the UE side for bistatic sensing to localize the UE as well as mapping the surrounding environment, and another PMB filter is run at the BS side for monostatic sensing to map the surrounding environment as well as the passive UE.

1) *Bistatic Sensing*: At the UE side,  $\mathcal{Z}_k^{\text{B}}$  is taken as input and a PMB SLAM filter is run to both track the UE and map the landmarks, i.e., VAs and SPs. We denote the map for bistatic sensing as  $\mathcal{X}^{\text{B}}$ . The goal of the PMB SLAM filter is to recursively compute the joint posterior  $f(\mathbf{s}_{k+1}^{\text{B}}, \mathcal{X}_{1:k+1}^{\text{B}} | \mathcal{Z}_{1:k+1}^{\text{B}})$  every time step, following the Bayesian filtering framework with RFSs [11]

$$f(\mathbf{s}_{k+1}^{\text{B}}, \mathcal{X}_{1:k+1}^{\text{B}} | \mathcal{Z}_{1:k+1}^{\text{B}}) \propto \ell(\mathcal{Z}_{k+1}^{\text{B}} | \mathbf{s}_{k+1}^{\text{B}}, \mathcal{X}^{\text{B}}) f(\mathcal{X}^{\text{B}} | \mathcal{Z}_{1:k}^{\text{B}}) \times \int f(\mathbf{s}_k | \mathcal{Z}_{1:k}^{\text{B}}) f(\mathbf{s}_{k+1} | \mathbf{s}_k) d\mathbf{s}_k, \quad (12)$$

where  $\ell(\mathcal{Z}_{k+1}^{\text{B}} | \mathbf{s}_{k+1}^{\text{B}}, \mathcal{X}^{\text{B}})$  denotes the RFS likelihood function of the measurement set of bistatic sensing, given by [24, eqs. (5)–(6)]. Instead of tracking the joint density, the marginal posteriors  $f(\mathbf{s}_k | \mathcal{Z}_{1:k}^{\text{B}})$  and  $f(\mathcal{X}_{1:k}^{\text{B}} | \mathcal{Z}_{1:k}^{\text{B}})$  are tracked by marginalizing out the map state and the UE state in the joint

posterior, respectively, described as

$$f(\mathbf{s}_{k+1}|\mathcal{Z}_{1:k+1}^B) = \int f(\mathbf{s}_{k+1}, \mathcal{X}^B|\mathcal{Z}_{1:k+1}^B)\delta\mathcal{X}^B, \quad (13)$$

$$f(\mathcal{X}^B|\mathcal{Z}_{1:k+1}^B) = \int f(\mathbf{s}_{k+1}, \mathcal{X}^B|\mathcal{Z}_{1:k+1}^B)d\mathbf{s}_{k+1}, \quad (14)$$

where  $\int \psi(\mathcal{X})\delta\mathcal{X}$  denotes the set integral [23, eq. (4)]. The EK-PMB SLAM filter proposed in [11] is used to solve the SLAM problem for bistatic sensing. Since there are different types of landmarks (VAs and SPs), a multi-model implementation of the filter is applied.

2) *Monostatic Sensing*: At the BS side,  $\mathcal{Z}_k^M$  is taken as input and a PMB filter is run to map the IPs as well as the passive UE. We denote the map for monostatic sensing as  $\mathcal{X}^M$ . This PMB filter is to recursively compute the posterior  $f(\mathcal{X}^M|\mathcal{Z}_{1:k+1}^M)$ , given by (for the IP map)

$$f(\mathcal{X}^M|\mathcal{Z}_{1:k+1}^M) \propto \ell(\mathcal{Z}_{k+1}^M|\mathcal{X}^M)f(\mathcal{X}^M|\mathcal{Z}_{1:k}^M), \quad (15)$$

where  $\ell(\mathcal{Z}_{k+1}^M|\mathcal{X}^M)$  denotes the RFS likelihood function of the measurement set of monostatic sensing. Since the UE may also reflect energy during monostatic sensing, a multi-model implementation is used, where possible IPs are treated as static landmarks, while the possible UE follows a random walk model as (3), leading to  $f(\mathcal{X}_{k+1}^M|\mathcal{Z}_{1:k+1}^M) \propto \ell(\mathcal{Z}_{k+1}^M|\mathcal{X}_{k+1}^M)f(\mathcal{X}_{k+1}^M|\mathcal{Z}_{1:k}^M)$  after prediction.

3) *Output of the Filters*: Note that (12)–(15) are implemented by the prediction and update steps of the PMB components (please refer to [11] for details). At the end of the two PMB filters, we have the following components:  $f^B(\mathbf{s}_k)$ ,  $\lambda_k^B(\mathbf{x})$  and  $\{r_k^{B,i}, \{w_{\zeta,k}^{B,i}, f_{\zeta,k}^{B,i}(\mathbf{x})\}_{\zeta \in \{\text{VA}, \text{SP}\}}\}_{i \in \mathbb{I}_k^B}$  for bistatic sensing, with  $w_{\zeta,k}^{B,i}$  and  $f_{\zeta,k}^{B,i}(\mathbf{x})$  representing the probability of the landmark type being  $\zeta \in \{\text{VA}, \text{SP}\}$  and its spatial density;  $f_k^M(\mathbf{x}_{\text{UE},k})$ ,  $\lambda_k^M(\mathbf{x})$  and  $\{r_k^{M,i}, f_k^{M,i}(\mathbf{x})\}_{i \in \mathbb{I}_k^M}$  for monostatic sensing, where  $f_k^M(\mathbf{x}_{\text{UE},k})$  is picked up from  $\mathcal{X}_k^M$  by taking the hard decision on the type and the rest are for  $\mathcal{X}^M$ .

#### IV. FUSION OF TWO SENSING MODALITIES

The two filters (one at the BS and one at the UE) run in parallel, based on the downlink signals sent by the BS. Periodically, the separate maps will be fused at the fusion center, which we assume is at the BS side, and the fused map is sent back to the BS and the UE. The operation of such fusion is described next. We drop the condition on measurement sets in this section for notation simplicity and consider the two individual filters at time step  $k$ . At the UE, from bistatic sensing, we have the UE posterior, denoted as  $f_k^B(\mathbf{s})$ , and the PMB  $f_k(\mathcal{X}^B)$  with components  $\lambda_k^B(\mathbf{x})$  and  $\{r_k^{B,i}, \{w_{\zeta,k}^{B,i}, f_{\zeta,k}^{B,i}(\mathbf{x})\}_{\zeta \in \{\text{VA}, \text{SP}\}}\}_{i \in \mathbb{I}_k^B}$ . At the BS, from monostatic sensing, we have  $f_k^M(\mathbf{x}_{\text{UE},k})$  and the PMB  $f_k(\mathcal{X}^M)$  with components  $\lambda_k^M(\mathbf{x})$  and  $\{r_k^{M,i}, f_k^{M,i}(\mathbf{x})\}_{i \in \mathbb{I}_k^M}$ . This section introduces map fusion and how the UE state density can be treated.

##### A. Map Fusion

To further reduce the notational burden, we will also omit the current time step  $k$ . Then, given  $f(\mathcal{X}^B)$  and  $f(\mathcal{X}^M)$ , we

aim to form a new map with PMB density  $f(\mathcal{X}^F)$ , which will be parameterized by  $\lambda^F(\mathbf{x})$  and  $\{r^{F,i}, f^{F,i}(\mathbf{x})\}_{i \in \mathbb{I}^F}$ . The process comprises two steps: map matching and component fusion. Note that the VAs and SPs in  $\mathcal{X}^B$  should be converted to IPs by modifying the corresponding densities, to be able to fuse with IPs in  $\mathcal{X}^M$ , where  $f_{\text{VA},k}^{B,i}(\mathbf{x})$  changes according to (4) and  $f_{\text{SP},k}^{B,i}(\mathbf{x})$  is unchanged.

1) *Map Matching*: The problem of matching Bernoullis can be cast as an optimal assignment problem [27], given by

$$\begin{aligned} \text{minimize} \quad & \text{tr}(\mathbf{A}^T \mathbf{C}) \\ \text{s.t.} \quad & a_{i,i'} \in \{0, 1\}, \quad \forall i, i', \\ & \sum_i a_{i,i'} \leq 1, \quad \forall i', \\ & \sum_{i'} a_{i,i'} = 1, \quad \forall i, \end{aligned} \quad (16)$$

where  $\mathbf{A} \in \mathbb{R}^{|\mathbb{I}^B| \times (|\mathbb{I}^M| + |\mathbb{I}^B|)}$  is the optimization variable and  $\mathbf{C} \in \mathbb{R}^{|\mathbb{I}^B| \times (|\mathbb{I}^M| + |\mathbb{I}^B|)}$  depends on the two PMBs. We define the cost matrix  $\mathbf{C}$  as

$$\mathbf{C} = \begin{bmatrix} c(1, 1) & \dots & c(1, |\mathbb{I}^M|) & | & T_G & \dots & \infty \\ \vdots & \ddots & \vdots & | & \vdots & \ddots & \vdots \\ c(|\mathbb{I}^B|, 1) & \dots & c(|\mathbb{I}^B|, |\mathbb{I}^M|) & | & \infty & \dots & T_G \end{bmatrix}, \quad (17)$$

where  $T_G$  is the gating threshold for matching Bernoullis, and  $c(i, i')$  is the cost of matching Bernoulli  $i$  in  $\mathcal{X}^B$  with Bernoulli  $i'$  in  $\mathcal{X}^M$ . The cost is defined as

$$c(i, i') = c(i, i', \zeta^*), \quad (18)$$

$\zeta^* \in \{\text{VA}, \text{SP}\}$  and  $c(i, i', \zeta^*)$  is now defined by

$$c(i, i', \zeta^*) = \frac{1}{2w_{\zeta^*}^{B,i}} (\|\xi_{\zeta^*}^{B,i} - \xi^{M,i'}\|_{\Sigma_{\zeta^*}^{B,i}} + \|\xi_{\zeta^*}^{B,i} - \xi^{M,i'}\|_{\Sigma^{M,i}}), \quad (19)$$

with  $\xi_{\zeta^*}^{B,i}$  and  $\Sigma_{\zeta^*}^{B,i}$  representing the mean and covariance of the converted density from  $f_{\text{VA}}^{B,i}(\mathbf{x})$  to an IP density according to (4) or the density  $f_{\text{SP}}^{B,i}(\mathbf{x})$ ,  $\xi^{M,i}$  and  $\Sigma^{M,i}$  representing the mean and covariance of  $f^{M,i}(\mathbf{x})$ , and  $\|\mathbf{x}\|_{\Sigma} = \mathbf{x}^T \Sigma^{-1} \mathbf{x}$ . Correspondingly, we introduce the decision on whether the landmark for the association  $(i, i')$  is a VA or a SP by

$$\zeta^* = \arg \min_{\zeta} \{c(i, i', \zeta)\}_{\zeta \in \{\text{VA}, \text{SP}\}}. \quad (20)$$

In (17), the left  $|\mathbb{I}^B| \times |\mathbb{I}^M|$  sub-matrix corresponds to matches of Bernoullis in  $\mathcal{X}^B$ , the right  $|\mathbb{I}^B| \times |\mathbb{I}^B|$  diagonal sub-matrix corresponds to mismatches of Bernoullis in  $\mathcal{X}^B$ . Solving this optimal assignment problem is the main computational cost of the fusion process, but it is much less costly than the mapping and SLAM filters, and can be solved efficiently by the Auction algorithm [27]. As a hard decision on the landmark type  $\zeta$  is made in (18) for each possible pair, the type of landmarks can be determined together with solving the optimal assignment problem.

2) *Component Fusion*: After map matching, there are several possibilities:

- *Match exists for  $f_{\zeta^*}^{B,i}(\mathbf{x})$* : In this case,  $f_{\zeta^*}^{B,i}(\mathbf{x})$  is matched to  $f^{M,i'}(\mathbf{x})$  for an  $i'$ . Appendix A shows how to obtain the fused Bernoulli. The same procedure applies to any

$f^{M,i}(\mathbf{x})$  for which a match exists. After fusion, the type of the corresponding landmark is determined. Therefore, that weight  $w_{\zeta^*}^{B,i}$  is set to 1, and another weight is set to 0 in  $\mathcal{X}^B$  for the multi-model implementation.

- *No match exists for  $f_{\zeta^*}^{B,i}(\mathbf{x})$* : In this case,  $f_{\zeta^*}^{B,i}(\mathbf{x})$  is not matched to any  $f^{M,i'}(\mathbf{x})$  for all  $i'$ . Appendix B shows how to obtain a Bernoulli by fusing  $f_{\zeta^*}^{B,i}(\mathbf{x})$  with the PPP  $\lambda^M(\mathbf{x})$ , where a hard decision is made on  $\zeta$  according to (20). A similar procedure exists for any  $f^{M,i}(\mathbf{x})$  for which no match exists.

After generating all Bernoullis in the fused map, we can re-index these Bernoullis, making  $i \in \mathbb{I}^F$ , so that  $\mathcal{X}^F$  is a MB with  $\{r^{F,i}, f^{F,i}(\mathbf{x})\}_{i \in \mathbb{I}^F}$ . The two PPPs are also fused, based on Appendix C. Finally,  $\mathcal{X}^B$  and  $\mathcal{X}^M$  are overwritten by  $\mathcal{X}^F$ . Note that some small modifications should be made when overwriting  $\mathcal{X}^B$  by  $\mathcal{X}^F$ . The spatial density of a VA should be recovered based on (4). A fused Bernoulli which is generated by fusing  $f^{M,i'}(\mathbf{x})$  with  $\lambda^B$ , should keep the multi-model representation with 50% of being SP and 50% of being VA in  $\mathcal{X}^B$ , as we are not sure the type of the corresponding landmark, and another spatial density can be generated by simply duplicating the density of the VA/SP according to (4).

### B. UE State Fusion

At time step  $k$ , the UE posterior  $f_k^B(\mathbf{s})$  provided by the EK-PMB SLAM filter at the UE side for bistatic sensing can be fused with the spatial density of the Bernoulli for the UE provided by the EK-PMB filter at the BS side for monostatic sensing, given by

$$f_k^F(\mathbf{s}_k) = \frac{f_k^B(\mathbf{s}_k) f_k^M(\mathbf{x}_{UE,k})}{\int f_k^B(\mathbf{s}'_k) f_k^M(\mathbf{x}'_{UE,k}) d\mathbf{s}'_k}, \quad (21)$$

since the UE serves as a passive object in monostatic sensing, which only provides information on the UE position, i.e.,  $\mathbf{x}_{UE,k} = [\mathbf{s}_k]_{1:3}$ . After fusion,  $f_k^B(\mathbf{s}_k)$  and  $f_k^M(\mathbf{x}_{UE,k})$  are overwritten by  $f_k^F(\mathbf{s}_k)$  and  $f_k^F(\mathbf{x}_{UE,k})$ .

## V. NUMERICAL RESULTS

### A. Simulation Environment

We consider the scenario introduced in [9], which is at 28 GHz and contains a single mmWave BS with a known location, and four VAs and four SPs with unknown locations. Additionally, there is a UE doing a counterclockwise constant turn-rate movement around the BS on the x-y plane, and its state is unknown. The BS and UE are both equipped with an  $8 \times 8$  omnidirectional URA. The BS broadcasts OFDM pilot signals with 16 symbols, 64 subcarriers, and 200 MHz bandwidth. Random precoders and combiners are used in both modalities. The transmitted power is set to 35 dBm. The noise figure at the BS is 20 dBm lower than the noise figure at the UE. The noise spectral density is -174 dBm/Hz. Path loss is generated according to [22, eq. (45)], with the reflection coefficient of reflecting surfaces and the radar cross-section of small objects as 0.7 and 50 m<sup>2</sup>, respectively. The Fisher information matrix of channel parameters [22] is used as the covariance in (7) and (8). The UE, VAs, and SPs are always

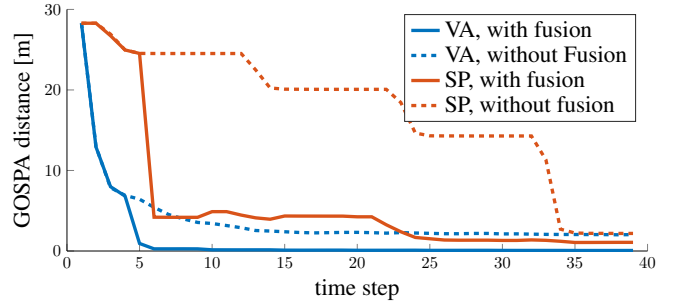


Fig. 2. Comparison of mapping performances for VAs and SPs in bistatic sensing between two cases: with and without fusion.

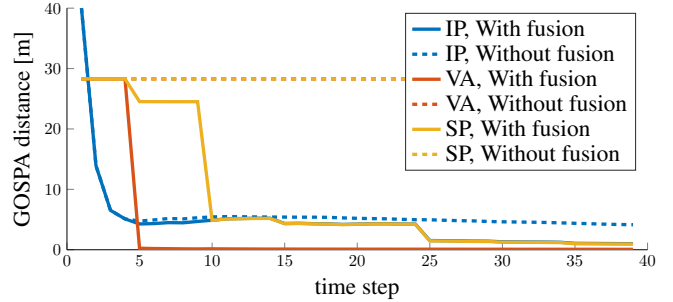


Fig. 3. Comparison of mapping performances for IPs, VAs, and SPs in monostatic sensing between two cases: with and without fusion.

visible to the BS. The BS and VAs are always visible to the UE, while SPs are only visible to the UE within the field of view of the UE, which is set as 50 m. The detection probability of each visible path is set as 0.9. The gating threshold  $T_G$  is set as 25.

The EK-PMB (SLAM) filters with considering 10 best DAs are implemented to solve the SLAM and mapping problems for bistatic and monostatic sensing. To evaluate the benefits of the integration of bistatic and monostatic sensing, we run two simulations: individual bistatic and monostatic sensing without any fusion, and bistatic and monostatic sensing with periodic map and UE state fusion. The simulations are run for one vehicle cycle, which is 40 time steps, and the fusion happens every 5 time steps. The mapping performance is evaluated by the generalized optimal subpattern assignment (GOSPA) distance [28] for both VAs and SPs for bistatic sensing, and for IPs, VAs and SPs for monostatic sensing. The positioning performance is quantified by the root mean squared error (RMSE). Overall, 100 Monte Carlo simulations are performed.

### B. Results

We first analyze how the integration of two sensing modalities affects the mapping performance. Fig. 2 compares the GOSPA distances between bistatic sensing with and without periodic fusion for VAs and SPs, and Fig. 3 compares the GOSPA distances between monostatic sensing with and without periodic fusion for IPs, VAs and SPs. Both figures demonstrate that the EK-PMB (SLAM) filter can map the landmarks in both sensing modalities and the mapping performance continuously increases with more measurements being



received, as GOSPA distances for VAs and SPs in Fig. 2 and IPs in Fig. 3 decrease over time. These figures also show that the type of landmarks can be distinguished accurately in bistatic sensing, which is due to the VAs and SPs generating measurements by following different observation models and the multi-model implementation of the EK-PMB SLAM filter proposed in [11] is utilized to solve this problem. However, we cannot distinguish landmark types in monostatic sensing, as landmarks are treated all the same as IPs. Moreover, the periodic fusion of two sensing modalities improves the mapping performances in both cases, as solid lines are always lower than dashed lines in both figures, which benefits from using information from both modalities, i.e., the fusion considers measurements at the UE side in bistatic sensing and measurements at the BS side in monostatic sensing, and the better UE positioning in bistatic sensing (see later). Especially, in bistatic sensing, SPs are detected sequentially due to the limited field of view of the UE to SPs, and all SPs can be detected until time step 34. This is also the reason why the red dashed line in Fig. 2 drops step by step, as the misdetection of these unseen SPs brings a penalty to the GOSPA distance, which remains until all unseen SPs are seen and detected. However, SPs are always visible to the BS, and the fusion with the monostatic sensing map introduces the unseen landmarks in bistatic sensing but detected in monostatic sensing to the bistatic sensing map, which makes the fused map detect all SPs after the first fusion at time step 5 and distinguish the unseen SPs types one step later. Therefore, the red solid line in Fig. 2 dramatically decreases at time step 6. The SP and VA GOSPA distances are provided merely to show that without fusion the BS has no way to distinguish the landmark type, leading to high GOSPA distances, but the fusion introduces the landmark types into the monostatic sensing map.

Finally, we validate the benefits of the integration of two sensing modalities in positioning performance. Fig. 4 displays the RMSEs of the estimated UE position, heading, and bias for both sensing modalities with and without fusion. From the figure, we observe that monostatic sensing can only estimate the UE position, and cannot estimate its heading and clock bias, as the UE serves as a passive object in monostatic sensing, while UE position, heading, and clock bias can be estimated in bistatic sensing, as channel parameters depend on all three terms. Bistatic sensing provides roughly four times better position estimates than monostatic sensing. This big gap is caused by the consideration of the UE movement model as well as the benefit of the mapping in bistatic sensing. However, monostatic sensing does not have a good UE movement model and all the rest measurements from other landmarks cannot contribute to UE positioning, as they do not contain any information on the UE state. Fig. 4 also displays that the periodic fusion can further improve the positioning performance in bistatic sensing, as all blue bars are lower than the red bars, indicating better position, heading and clock bias estimations can be acquired. The reason is that a better map can be obtained by the periodic fusion of two maps and measurements from the passive UE in monostatic sensing are also used, which benefit the UE positioning. Please note that the better UE positioning can also enhance the mapping

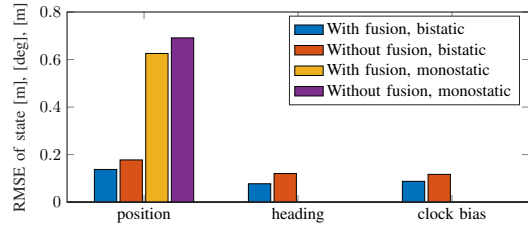


Fig. 4. Comparison of UE state estimation in bistatic and monostatic sensing between two cases: with and without fusion.

performance in turn. With periodic fusion, monostatic sensing can also obtain better UE position estimates. This is because the estimation error drops when the fusion happens and is more or less the same as before for the rest time steps.

## VI. CONCLUSIONS

In this paper, we address the SLAM problem in bistatic sensing and the mapping problem in monostatic sensing using EK-PMB (SLAM) filters. A RFS-based algorithm for integrating monostatic and bistatic sensing is first introduced in this paper, and executable details on the fusion of maps and UE states are also provided. Via simulations, which use realistic mmWave signal parameters, we demonstrate that the implementation of the EK-PMB (SLAM) filters can map the environment and position the UE state simultaneously in bistatic sensing, and map the environment as well as the passive UE in monostatic sensing. The results also indicate that periodic fusion of monostatic and bistatic sensing helps the filters to acquire better mapping and SLAM performances in monostatic and bistatic sensing, respectively.

## ACKNOWLEDGMENTS

This work was supported, in part, by the Wallenberg AI, Autonomous Systems and Software Program (WASP) funded by Knut and Alice Wallenberg Foundation, by Hexa-X-II, part of the European Union’s Horizon Europe research and innovation programme under Grant Agreement No 101095759, and by the Basic Science Research Program through the National Research Foundation of Korea (2022R1A6A3A03068510).

## APPENDIX MAP FUSION

### A. Fusion of Two Bernoullis

By following the generalized covariance intersection (GCI) approach, the fusion of two Bernoullis  $\{r^B, f^B(\mathbf{x})\}$  and  $\{r^M, f^M(\mathbf{x})\}$  results in a Bernoulli with parameters [29]–[31]

$$r^F = \frac{C(r^B)^\alpha (r^M)^\beta}{C(r^B)^\alpha (r^M)^\beta + (1 - r^B)^\alpha (1 - r^M)^\beta}, \quad (22)$$

$$f^F(\mathbf{x}) = \frac{f^B(\mathbf{x})^\alpha f^M(\mathbf{x})^\beta}{C}, \quad (23)$$

where  $C = \int f^B(\mathbf{x})^\alpha f^M(\mathbf{x})^\beta d(\mathbf{x})$ ,  $\alpha$  and  $\beta$  are the fusion weights, satisfying  $\alpha + \beta = 1$ , with  $\alpha = r^B / (r^B + r^M)$ , and  $\beta = r^M / (r^B + r^M)$ .

## B. Fusion of a Bernoulli with a PPP

The fusion of a Bernoulli  $\{r^B, f^B(\mathbf{x})\}$  and a PPP  $\lambda^M(\mathbf{x}) = \eta^M f_P^M$  results in a Bernoulli with parameters [31]

$$r^F = \frac{C(r^B)^\alpha (\eta^M)^\beta}{C(r^B)^\alpha (\eta^M)^\beta + (1 - r^B)^\alpha}, \quad (24)$$

$$f^F(\mathbf{x}) = \frac{f^B(\mathbf{x})^\alpha f_P^M(\mathbf{x})^\beta}{C}, \quad (25)$$

with  $C = \int f^B(\mathbf{x})^\alpha f_P^M(\mathbf{x})^\beta d(\mathbf{x})$ ,  $\alpha = r^B / (r^B + \eta^M)$ , and  $\beta = r^M / (r^B + \eta^M)$ .

## C. Fusion of two PPPs

Fusion of two PPPs  $\lambda^B(\mathbf{x}) = \eta^B f_P^B$  and  $\lambda^M(\mathbf{x}) = \eta^M f_P^M$  results in a new PPP with parameters [31]

$$\lambda^F(\mathbf{x}) = \lambda^B(\mathbf{x})^\alpha \lambda^M(\mathbf{x})^\beta = \eta^F f_P^F(\mathbf{x}), \quad (26)$$

$$\eta^F = C(\eta^B)^\alpha (\eta^M)^\beta, \quad (27)$$

$$f_P^F(\mathbf{x}) = \frac{f_P^B(\mathbf{x})^\alpha f_P^M(\mathbf{x})^\beta}{C}, \quad (28)$$

where  $C = \int f_P^B(\mathbf{x})^\alpha f_P^M(\mathbf{x})^\beta d(\mathbf{x})$ , and  $\alpha = \beta = 1/2$ .

## REFERENCES

- [1] A. Liu, Z. Huang, M. Li, Y. Wan, W. Li, T. X. Han, C. Liu, R. Du, D. K. P. Tan, J. Lu, *et al.*, "A survey on fundamental limits of integrated sensing and communication," *IEEE Commun. Surv. Tutor.*, vol. 24, no. 2, pp. 994–1034, 2022.
- [2] C. Chaccour, M. N. Soorki, W. Saad, M. Bennis, P. Popovski, and M. Debbah, "Seven defining features of terahertz (THz) wireless systems: A fellowship of communication and sensing," *IEEE Communications Surveys & Tutorials*, vol. 24, no. 2, pp. 967–993, 2022.
- [3] Y. Ge, O. Kaltiokallio, H. Kim, J. Talvitie, S. Kim, L. Svensson, M. Valkama, and H. Wymeersch, "Mmwave mapping and SLAM for 5G and beyond," in *Integrated Sensing and Communications*. Springer, 2023, pp. 445–475.
- [4] D. Crouse, "Basic tracking using nonlinear 3D monostatic and bistatic measurements," *IEEE Aerospace and Electronic Systems Magazine*, vol. 29, no. 8, pp. 4–53, 2014.
- [5] P. Stinco and F. Gini, "Performance analysis of bistatic radar and optimization methodology in multistatic radar system," *University of Pisa, Pisa*, 2012.
- [6] A. Yassin, Y. Nasser, A. Y. Al-Dubai, and M. Awad, "MOSAIC: Simultaneous localization and environment mapping using mmwave without a-priori knowledge," *IEEE Access*, vol. 6, pp. 68 932–68 947, 2018.
- [7] H. Zhang, B. Di, K. Bian, Z. Han, H. V. Poor, and L. Song, "Toward ubiquitous sensing and localization with reconfigurable intelligent surfaces," *Proceedings of the IEEE*, vol. 110, no. 9, pp. 1401–1422, 2022.
- [8] E. Leitinger, F. Meyer, F. Hlawatsch, K. Witrissal, F. Tufvesson, and M. Z. Win, "A belief propagation algorithm for multipath-based SLAM," *IEEE Trans. Wireless Commun.*, vol. 18, no. 12, pp. 5613–5629, Sep. 2019.
- [9] O. Kaltiokallio, Y. Ge, J. Talvitie, H. Wymeersch, and M. Valkama, "mmWave simultaneous localization and mapping using a computationally efficient EK-PHD filter," in *IEEE International Conference on Information Fusion (Fusion)*, 2021, pp. 1–6.
- [10] H. Kim, H. Chen, M. F. Keskin, Y. Ge, K. Keykhosravi, G. C. Alexandropoulos, S. Kim, and H. Wymeersch, "RIS-enabled and access-point-free simultaneous radio localization and mapping," *arXiv preprint arXiv:2212.07141*, 2022.
- [11] Y. Ge, O. Kaltiokallio, H. Kim, F. Jiang, J. Talvitie, M. Valkama, L. Svensson, S. Kim, and H. Wymeersch, "A computationally efficient EK-PMBM filter for bistatic mmWave radio SLAM," *IEEE Journal on Selected Areas in Communications*, 2022.
- [12] E. Denove, "Multiple target tracking in experimental multistatic MIMO mmWave radar sensor networks," Ph.D. dissertation, Massachusetts Institute of Technology, 2021.
- [13] H. Kim, A. Fascista, H. Chen, Y. Ge, G. C. Alexandropoulos, G. Seco-Granados, and H. Wymeersch, "RIS-aided radar sensing and object detection with single and double bounce multipath," *arXiv preprint arXiv:2212.07142*, 2022.
- [14] J. Yang, C.-K. Wen, and S. Jin, "Hybrid active and passive sensing for SLAM in wireless communication systems," *IEEE Journal on Selected Areas in Communications*, vol. 40, no. 7, pp. 2146–2163, 2022.
- [15] J. Palacios, G. Bielsa, P. Casari, and J. Widmer, "Single-and multiple-access point indoor localization for millimeter-wave networks," *IEEE Trans. Wireless Commun.*, vol. 18, no. 3, pp. 1927–1942, 2019.
- [16] R. W. Heath, N. Gonzalez-Prelcic, S. Rangan, W. Roh, and A. M. Sayeed, "An overview of signal processing techniques for millimeter wave MIMO systems," *IEEE Journal of Selected Topics in Signal Processing*, vol. 10, no. 3, pp. 436–453, 2016.
- [17] Y. Ge, F. Wen, H. Kim, M. Zhu, F. Jiang, S. Kim, L. Svensson, and H. Wymeersch, "5G SLAM using the clustering and assignment approach with diffuse multipath," *Sensors (Basel, Switzerland)*, vol. 20, no. 16, August 2020. [Online]. Available: <https://doi.org/10.3390/s20164656>
- [18] A. Richter, "Estimation of radio channel parameters: Models and algorithms," Ph.D. dissertation, Ilmenau University of Technology, 2005.
- [19] K. Venugopal, A. Alkhateeb, N. G. Prelcic, and R. W. Heath, "Channel estimation for hybrid architecture-based wideband millimeter wave systems," *IEEE Journal on Selected Areas in Communications*, vol. 35, no. 9, pp. 1996–2009, 2017.
- [20] A. B. Gershman, M. Rubsamen, and M. Pesavento, "One- and two-dimensional direction-of-arrival estimation: An overview of search-free techniques," *Signal Processing*, vol. 90, no. 5, pp. 1338 – 1349, 2010.
- [21] F. Jiang, F. Wen, Y. Ge, M. Zhu, H. Wymeersch, and F. Tufvesson, "Beamspace multidimensional ESPRIT approaches for simultaneous localization and communications," *arXiv preprint arXiv:2111.07450*, 2021.
- [22] Z. Abu-Shaban, X. Zhou, T. Abhayapala, G. Seco-Granados, and H. Wymeersch, "Error bounds for uplink and downlink 3D localization in 5G millimeter wave systems," *IEEE Transactions on Wireless Communications*, vol. 17, no. 8, pp. 4939–4954, 2018.
- [23] J. L. Williams, "Marginal multi-Bernoulli filters: RFS derivation of MHT, JIPDA, and association-based MeMBer," *IEEE Transactions on Aerospace and Electronic Systems*, vol. 51, no. 3, pp. 1664–1687, 2015.
- [24] . F. Garca-Fernandez, J. L. Williams, K. Granstrom, and L. Svensson, "Poisson multi-Bernoulli mixture filter: Direct derivation and implementation," *IEEE Transactions on Aerospace and Electronic Systems*, vol. 54, no. 4, pp. 1883–1901, 2018.
- [25] M. Fatemi, K. Granstrom, L. Svensson, F. J. Ruiz, and L. Hammarstrand, "Poisson multi-Bernoulli mapping using Gibbs sampling," *IEEE Transactions on Signal Processing*, vol. 65, no. 11, pp. 2814–2827, 2017.
- [26] R. P. Mahler, *Advances in Statistical Multisource-Multitarget Information Fusion*. Artech House, 2014.
- [27] S. S. Blackman and R. Popoli, *Design and analysis of modern tracking systems*. Artech House, 1999.
- [28] A. S. Rahmathullah, . F. Garca-Fernandez, and L. Svensson, "Generalized optimal sub-pattern assignment metric," in *20th IEEE International Conference on Information Fusion (Fusion)*, 2017.
- [29] R. P. Mahler, "Optimal/robust distributed data fusion: A unified approach," in *Signal Processing, Sensor Fusion, and Target Recognition IX*, vol. 4052. SPIE, 2000, pp. 128–138.
- [30] G. Battistelli, L. Chisci, C. Fantacci, A. Farina, and A. Graziano, "Consensus CPHD filter for distributed multitarget tracking," *IEEE J. Sel. Topics Signal Process.*, vol. 7, no. 3, pp. 508–520, Jun 2013.
- [31] M. Frohle, K. Granstrom, and H. Wymeersch, "Decentralized Poisson multi-Bernoulli filtering for vehicle tracking," *IEEE Access*, vol. 8, pp. 126 414–126 427, 2020.